Casimir-Polder shift and decay rate in the presence of nonreciprocal media

Sebastian Fuchs,[1] J. A. Crosse,[2] and Stefan Yoshi Buhmann[1,3]

[1]*Physikalisches Institut, Albert-Ludwigs-Universität Freiburg, Hermann-Herder-Straße 3, 79104 Freiburg, Germany*

[2]*Department of Electrical and Computer Engineering, National University of Singapore, 4 Engineering Drive 3, 117583, Singapore*

[3]*Freiburg Institute for Advanced Studies, Albert-Ludwigs-Universität Freiburg, Albertstraße 19, 79104 Freiburg, Germany*

(Received 19 May 2016; published 2 February 2017)

We calculate the Casimir–Polder frequency shift and decay rate for an atom in front of a nonreciprocal medium by using macroscopic quantum electrodynamics. The results are a generalization of the respective quantities for matter with broken time-reversal symmetry which does not fulfill the Lorentz reciprocity principle. As examples, we contrast the decay rates, the resonant and nonresonant frequency shifts of a perfectly conducting (reciprocal) mirror with those of a perfectly reflecting nonreciprocal mirror. We find different power laws for the distance dependence of all quantities in the retarded and nonretarded limits. As an example of a more realistic nonreciprocal medium, we investigate a topological insulator subject to a time-symmetry-breaking perturbation.

DOI: 10.1103/PhysRevA.95.023805

I. INTRODUCTION

The Casimir–Polder force [1], like the van der Waals and the Casimir forces [2], is a dispersion force [3,4]. This weak electromagnetic force was studied by using a variety of different methods. The lifetime and the frequency shift of an atom in its ground state or excited state near a flat surface, which causes the Casimir–Polder force, are analyzed by using a quantum-mechanical linear-response formalism in Refs. [5,6]. This is exemplified for a perfect conductor and a metal plate.

The Casimir–Polder force can also be viewed as result of noise currents composed of noise polarization and noise magnetization in matter, which act as a source for a quantized electromagnetic field. These fields can be expanded in terms of the classical electromagnetic Green's tensor for the Helmholtz equation [7–12]. By computing the interaction of an atom with this field one can compute the effect of material bodies on the internal properties of the atom. The Casimir–Polder force is a result of the level shift of the atom induced by this field. In this theoretical framework, materials are described macroscopically by electromagnetic physical quantities and therefore this approach is known as macroscopic quantum electrodynamics (QED) [3,4,13]. Casimir–Polder potentials have been investigated for graphene [14], metamaterials [15,16], and Rydberg atoms near metallic surfaces [17].

In bi-isotropic media electric and magnetic fields are coupled to each other and the general expressions of the constitutive relations read $\mathbf{D} = \varepsilon_0 \boldsymbol{\epsilon} \star \mathbf{E} + \frac{1}{c}\boldsymbol{\xi} \star \mathbf{H}$ and $\mathbf{B} = \frac{1}{c}\boldsymbol{\zeta} \star \mathbf{E} + \mu_0 \boldsymbol{\mu} \star \mathbf{H}$ (where $\star$ denotes a spatial convolution) with the cross susceptibilities $\boldsymbol{\xi}$ and $\boldsymbol{\zeta}$. If a material shows imaginary cross susceptibilities, the material is called chiral [18,19]. The radiation of a dipole in proximity to a thin [20] and a thick chiral layer [21] has already been studied. References [22,23] study the interaction between a chiral molecule in front of a chiral half space [23] and a chiral nanosphere [22]. The decay rate of spontaneous emission is computed in a direct way by using the electric and magnetic dipole moments, their induced counterparts, and the respective fields.

A bi-isotropic medium is called nonreciprocal if the mixing parameters have a real-valued contribution, e.g., a topological insulator which breaks time-reversal symmetry. In the theory of macroscopic QED, Lorentz's reciprocity principle stating the reversibility of optical paths, i.e., the symmetry with respect to an exchange of positions and orientations of sources and fields, holds for reciprocal material (Lorentz reciprocity being a particular case of the Onsager reciprocity from statistical physics [24]). Thus these materials preserve time-reversal symmetry. To study Casimir–Polder potentials for nonreciprocal media, which violate Lorentz's reciprocity relation [25], the theory of macroscopic QED was generalized to include these cross susceptibilities [26]. In this paper, we investigate the Casimir–Polder frequency shift and decay rate for a nonreciprocal medium.

Topological insulators [27–29] are time-symmetric materials which are characterized by an insulating bulk and protected conducting surface states and have been observed in three-dimensional (3D) materials which exhibit sufficiently strong spin-orbit coupling to induce band inversion [30]. These materials can be used to realize axion media. To do this one needs to introduce a time-reversal-symmetry-breaking perturbation to the surface, either via ferromagnetic dopants [31,32] or an external static magnetic field [33]. Such a perturbation opens a gap on the surface, converting the surface conductor into a full insulator and leads to a nontrivial electromagnetic response—in particular the electric and the magnetic fields $\mathbf{E}$ and $\mathbf{B}$ are able to mix [31].

This magneto-electric effect can be described by adding an axion Lagrangian density term $\mathscr{L}_{\text{axion}} = \alpha/(4\pi^2)\theta(\mathbf{r},\boldsymbol{\omega})\mathbf{E}\cdot\mathbf{B}$ to the usual electromagnetic Lagrangian density [34]. Here, α is the fine-structure constant and $\theta(\mathbf{r},\boldsymbol{\omega})$ is the space- and time-dependent axion coupling. The axion coupling θ vanishes in a trivial insulator but takes odd integer values of π in a time-reversal-symmetry-broken topological insulator, with the value and sign of the integer related to the strength and direction of the time-symmetry-breaking perturbation. Physically, this describes a quantum Hall effect on the surface of the topological insulator [31]. The lowest Hall plateau leads to an axion coupling of $\pm\pi$. Changing the size of the perturbation will not change the axion coupling until the next Hall plateau is reached, whereupon the axion coupling will increase to $\pm 3\pi$. Further changes to the perturbation would result in even higher axion couplings as the relevant Hall plateaus are reached. It has been previously shown that the mixing of the electric and magnetic fields by the axion coupling

has a significant effect on the Casimir force [35] and, as we will show in Sec. IV, it also modifies the Casimir–Polder shift.

Optical properties, e.g., reflective and transmissive properties, Fresnel formulas, Brewster angle, and the Goos–Hänchen effect of these materials have been studied theoretically in Refs. [36,37]. Reference [38] derives electric fields and dipole moments for stratified isorefractive Tellegen media (purely-real-valued coupling parameter between electric and magnetic field) with the Green's tensor method. One consequence of isorefractive media is the parallelism of the incident and transmitted beam. As for layered topological insulators with a time-reversal-symmetry-breaking perturbation, potential applications are broad; for example, a waveguide that induces polarization rotations due to the magneto-electric effect and mixes the electric and magnetic induction fields at the material's surface [39].

In our context, Casimir repulsion is of specific interest, e.g., the Casimir repulsion for magnetodielectric metamaterials predicted in Refs. [40–42]. Specifically, repulsive dispersion forces for a setup containing topological insulators are discussed in Ref. [35], such as Casimir forces between three-dimensional topological insulators. Based on this approach, it is shown in Ref. [43] that there is a critical band gap where the Casimir force switches from attractive to repulsive. The influence of unusual material properties, such as those of the topological insulator, on dispersion forces is emphasized in the recent review [44]. The Casimir–Polder interaction between an atom and a graphene surface with an applied magnetic field is studied in Ref. [45]. The authors observe plateau-like discontinuities of the Casimir–Polder interaction energy for specific values of the magnetic field and at low temperatures. This effect is traced back to the quantum Hall effect and is thus closely connected to our approach. We are going to apply the extended theory of macroscopic QED for nonreciprocal media to calculate frequency shifts and atomic decay rates of an atom in front of a topological insulator by directly using the electromagnetic properties derived in Ref. [46].

This paper on the Casimir–Polder shift and decay rate in the presence of nonreciprocal media is organized as follows: The time-dependent electric field is calculated in the framework of macroscopic QED for nonreciprocal media in Sec. II. This result is reached alternatively by a direct quantization of the noise current or by expressing noise polarization and magnetization through electromagnetic response functions and is needed for studying the internal atomic dynamics. This is described in Sec. III where the modified equations for the frequency shift and decay rate for nonreciprocal media are presented. In Sec. IV, the results are applied to a perfectly reflecting nonreciprocal mirror and a topological insulator described by an axion coupling. In this context, we distinguish between a pure nonreciprocal topological insulator and material properties similar to Bi_2Se_3. Finally, we discuss the possibility of switching between an attractive and a repulsive force.

II. THE TIME-DEPENDENT ELECTRIC FIELD

A nonreciprocal medium violates time-reversal symmetry and, hence, the Lorentz reciprocity principle for the Green's tensor [25] does not hold

$$\mathbf{G}^{\mathrm{T}}(\mathbf{r}',\mathbf{r},\boldsymbol{\omega}) \neq \mathbf{G}(\mathbf{r},\mathbf{r}',\boldsymbol{\omega}). \tag{1}$$

This necessitates new definitions for the real and imaginary parts of the Green's tensor $\mathbf{G}$

$$\mathcal{R}[\mathbf{G}(\mathbf{r},\mathbf{r}')] = \frac{1}{2}[\mathbf{G}(\mathbf{r},\mathbf{r}') + \mathbf{G}^{*\mathrm{T}}(\mathbf{r}',\mathbf{r})], \tag{2}$$

$$\mathcal{I}[\mathbf{G}(\mathbf{r},\mathbf{r}')] = \frac{1}{2i}[\mathbf{G}(\mathbf{r},\mathbf{r}') - \mathbf{G}^{*\mathrm{T}}(\mathbf{r}',\mathbf{r})]. \tag{3}$$

Thus the violation of Lorentz's principle calls for a modified mathematical description of macroscopic quantum electrodynamics (QED) for nonreciprocal media. Whereas the framework of macroscopic QED is described in Refs. [3,13], the modified approach for nonreciprocal media is outlined in Ref. [26]. The internal dynamics of an atom with reciprocal media is discussed in Refs. [4,8].

The general expression for the electric field reads

$$\hat{\mathbf{E}}(\mathbf{r}) = \int_0^\infty d\boldsymbol{\omega}[\hat{\mathbf{E}}(\mathbf{r},\boldsymbol{\omega}) + \hat{\mathbf{E}}^\dagger(\mathbf{r},\boldsymbol{\omega})], \tag{4}$$

with frequency components in Fourier space

$$\begin{aligned}\hat{\mathbf{E}}(\mathbf{r},\boldsymbol{\omega}) &= i\mu_0\boldsymbol{\omega}[\mathbf{G} \star \hat{\mathbf{j}}_{\mathrm{N}}](\mathbf{r},\boldsymbol{\omega}) \\ &= i\mu_0\boldsymbol{\omega}\int d^3r'\mathbf{G}(\mathbf{r},\mathbf{r}',\boldsymbol{\omega})\cdot\hat{\mathbf{j}}_{\mathrm{N}}(\mathbf{r}',\boldsymbol{\omega}),\end{aligned} \tag{5}$$

where $\star$ denotes a spatial convolution. The noise current density $\hat{\mathbf{j}}_{\mathrm{N}}$ is governed by the quantum fluctuations occurring in the medium and its average vanishes $\langle\hat{\mathbf{j}}_{\mathrm{N}}\rangle = \mathbf{0}$. $\hat{\mathbf{j}}_{\mathrm{N}}$ can either be quantized directly, as is outlined in Sec. II A, or it can be represented by noise polarization $\hat{\mathbf{P}}_{\mathrm{N}}$ and magnetization $\hat{\mathbf{M}}_{\mathrm{N}}$ and the respective electric and magnetic fields are quantized separately yielding creation and annihilation operators for each field. We dedicate Sec. II B to the second method using electric and magnetic response functions.

To obtain an expression for the time-dependent electric field (4), we have to find a solution for the time-dependent creation and annihilation operators first. This procedure is carried out both for a noise-current-based schema and a polarization-magnetization-founded method. The Hamiltonian $\hat{H}$ for the atom-field system is composed of the atomic part $\hat{H}_{\mathrm{A}}$, the field part $\hat{H}_{\mathrm{F}}$, and a contribution for the atom-field interaction $\hat{H}_{\mathrm{AF}}$: $\hat{H} = \hat{H}_{\mathrm{A}} + \hat{H}_{\mathrm{F}} + \hat{H}_{\mathrm{AF}}$. The atomic part $\hat{H}_{\mathrm{A}}$,

$$\hat{H}_{\mathrm{A}} = \sum_n E_n\hat{A}_{nn}, \tag{6}$$

incorporates the eigenenergy E_n for each atomic energy level and the atomic flip operator $\hat{A}_{mn} = |m\rangle\langle n|$. Resembling a harmonic oscillator, $\hat{H}_{\mathrm{F}}$ comprises the integral over all the frequency-dependent number operators of the field-medium system and can be cast in the two aforementioned ways; cf. Secs. II A and II B. The interaction Hamiltonian $\hat{H}_{\mathrm{AF}}$, which couples the atomic dipole to the electromagnetic field, reads

$$\hat{H}_{\mathrm{AF}} = -\hat{\mathbf{d}}\cdot\hat{\mathbf{E}}(\mathbf{r}_A) = -\sum_{m,n}\hat{A}_{mn}\mathbf{d}_{mn}\cdot\hat{\mathbf{E}}(\mathbf{r}_A) \tag{7}$$

and contains the electric-dipole operator $\hat{\mathbf{d}} = \sum_{m,n}\mathbf{d}_{mn}\hat{A}_{mn}$. $\mathbf{r}_{\mathrm{A}}$ is the position of the atom. Since $\hat{H}_{\mathrm{A}}$ commutes with the field operators, only the commutation relations for the field

Hamiltonian $\hat{H}_{\mathrm{F}}$ and the interaction Hamiltonian $\hat{H}_{\mathrm{AF}}$ have to be studied to find the expression for the electric field (4). The field operators' equations of motion will be solved in the two different ways and inserted into Eq. (5), thus giving a final expression for the electric field in the presence of an atom.

A. Electric field in noise-current-based schema

In this first approach, the noise current is quantized directly by expressions for the field operators. Ohm's Law in frequency space,

$$\hat{\mathbf{j}}_{\mathrm{in}}(\mathbf{r},\boldsymbol{\omega}) = [\mathbf{Q} \star \hat{\mathbf{E}}](\mathbf{r},\boldsymbol{\omega}) + \hat{\mathbf{j}}_{\mathrm{N}}(\mathbf{r},\boldsymbol{\omega}), \tag{8}$$

describes the effect of the electric field $\hat{\mathbf{E}}(\mathbf{r},\boldsymbol{\omega})$ on a linearly responding medium where $\mathbf{Q}$ is the conductivity matrix. Hence, the Helmholtz equation reads

$$\left[\overrightarrow{\nabla} \times \overrightarrow{\nabla} \times - \frac{\boldsymbol{\omega}^2}{c^2}\right]\mathbf{G}(\mathbf{r},\mathbf{r}',\boldsymbol{\omega}) - i\mu_0\boldsymbol{\omega}[\mathbf{Q} \star \mathbf{G}](\mathbf{r},\mathbf{r}'\boldsymbol{\omega}) = \boldsymbol{\delta}(\mathbf{r}-\mathbf{r}'). \tag{9}$$

This equation is formally solved by the Green's tensor $\mathbf{G}$ with $\mathbf{G} \to \mathbf{0}$ for $|\mathbf{r}-\mathbf{r}'| \to \infty$.

We quantize the noise-current density $\hat{\mathbf{j}}_{\mathrm{N}}$ in Eq. (5) directly by writing it in terms of creation and annihilation operators $\hat{\mathbf{f}}^{\dagger}$ and $\hat{\mathbf{f}}$

$$\hat{\mathbf{j}}_{\mathrm{N}}(\mathbf{r},\boldsymbol{\omega}) = \sqrt{\frac{\hbar\boldsymbol{\omega}}{\pi}}[\mathbf{R} \star \hat{\mathbf{f}}](\mathbf{r},\boldsymbol{\omega}), \tag{10}$$

where $\mathbf{R}$ is related to the real part of the conductivity tensor $\mathbf{Q}$

$$[\mathbf{R} \star \mathbf{R}^{*\mathrm{T}}](\mathbf{r},\mathbf{r}',\boldsymbol{\omega}) = \mathcal{R}[\mathbf{Q}(\mathbf{r},\mathbf{r}',\boldsymbol{\omega})]. \tag{11}$$

The Heisenberg equation of motion for the annihilation operator $\hat{\mathbf{f}}$

$$\dot{\hat{\mathbf{f}}}(\mathbf{r},\boldsymbol{\omega}) = \frac{1}{i\hbar}[\hat{\mathbf{f}}(\mathbf{r},\boldsymbol{\omega}),\hat{H}], \tag{12}$$

upon using the field Hamiltonian $\hat{H}_{\mathrm{F}}$,

$$\hat{H}_{\mathrm{F}} = \int d^3r \int_0^{\infty} d\boldsymbol{\omega}\hbar\boldsymbol{\omega}\hat{\mathbf{f}}^{\dagger}(\mathbf{r},\boldsymbol{\omega}) \cdot \hat{\mathbf{f}}(\mathbf{r},\boldsymbol{\omega}), \tag{13}$$

and the interaction Hamiltonian $\hat{H}_{\mathrm{AF}}$ (7) by using Eq. (5),

$$\hat{H}_{\mathrm{AF}} = -\sum_{m,n}\int_0^{\infty} d\boldsymbol{\omega} i\mu_0\boldsymbol{\omega}\sqrt{\frac{\hbar\boldsymbol{\omega}}{\pi}}\hat{A}_{mn}\mathbf{d}_{mn} \times \{[\mathbf{G} \star \mathbf{R} \star \hat{\mathbf{f}}](\mathbf{r}_A,\boldsymbol{\omega}) - [\mathbf{G}^* \star \mathbf{R}^* \star \hat{\mathbf{f}}^{\dagger}](\mathbf{r}_A,\boldsymbol{\omega})\}, \tag{14}$$

gives the solution of the annihilation operator $\hat{\mathbf{f}}$

$$\hat{\mathbf{f}}(\mathbf{r},\boldsymbol{\omega},t) = e^{-i\boldsymbol{\omega}(t-t_0)}\hat{\mathbf{f}}(\mathbf{r},\boldsymbol{\omega}) + \frac{\mu_0\boldsymbol{\omega}}{\hbar}\sqrt{\frac{\hbar\boldsymbol{\omega}}{\pi}}\sum_{m,n}\int_{t_0}^{t} dt' \times e^{-i\boldsymbol{\omega}(t-t')}[\mathbf{G} \star \mathbf{R}]^{*\mathrm{T}}(\mathbf{r}_A,\mathbf{r},\boldsymbol{\omega}) \cdot \mathbf{d}_{mn}\hat{A}_{mn}. \tag{15}$$

Substituting the results into Eq. (10) and using Eq. (11) and the expression

$$\mathcal{I}[\mathbf{G}(\mathbf{r},\mathbf{r}',\boldsymbol{\omega})] = \mu_0\boldsymbol{\omega}[\mathbf{G} \star \mathcal{R}[\mathbf{Q}] \star \mathbf{G}^{*\mathrm{T}}](\mathbf{r},\mathbf{r}',\boldsymbol{\omega}), \tag{16}$$

leads to an expression for the electric field in nonreciprocal media

$$\hat{\mathbf{E}}(\mathbf{r},\boldsymbol{\omega},t) = e^{-i\boldsymbol{\omega}(t-t_0)}\hat{\mathbf{E}}(\mathbf{r},\boldsymbol{\omega}) + i\frac{\mu_0\boldsymbol{\omega}^2}{\pi}\sum_{m,n}\int_{t_0}^{t} dt' \times e^{-i\boldsymbol{\omega}(t-t')}\mathcal{I}[\mathbf{G}(\mathbf{r},\mathbf{r}_A,\boldsymbol{\omega})] \cdot \mathbf{d}_{mn}\hat{A}_{mn}, \tag{17}$$

which differs from the usual expression for reciprocal media only by the definition of the imaginary part of the Green's tensor (3) [4].

B. Electric field in polarization-magnetization-based schema

The components of the electric field $\hat{\mathbf{E}}(\mathbf{r},\boldsymbol{\omega})$ can also be calculated in terms of electric and magnetic response functions, i.e., polarization and magnetization [26]. The constitutive relations for the electric displacement field $\hat{\mathbf{D}}$ and the magnetic induction field $\hat{\mathbf{B}}$ are given by [26]

$$\hat{\mathbf{D}} = \varepsilon_0\boldsymbol{\epsilon} \star \hat{\mathbf{E}} + \frac{1}{c}\boldsymbol{\xi} \star \hat{\mathbf{H}} + \hat{\mathbf{P}}_{\mathrm{N}} + \frac{1}{c}\boldsymbol{\xi} \star \hat{\mathbf{M}}_{\mathrm{N}}, \tag{18}$$

$$\hat{\mathbf{B}} = \frac{1}{c}\boldsymbol{\zeta} \star \hat{\mathbf{E}} + \mu_0\boldsymbol{\mu} \star \hat{\mathbf{H}} + \mu_0\boldsymbol{\mu} \star \hat{\mathbf{M}}_{\mathrm{N}}, \tag{19}$$

where the tensor $\boldsymbol{\epsilon}$ is the permittivity, $\boldsymbol{\mu}$ is the permeability and $\boldsymbol{\xi}$ and $\boldsymbol{\zeta}$ represent the magneto-electric cross susceptibilities. The noise polarization $\hat{\mathbf{P}}_{\mathrm{N}}$ and noise magnetization $\hat{\mathbf{M}}_{\mathrm{N}}$ form the noise current $\hat{\mathbf{j}}_{\mathrm{N}}$

$$\hat{\mathbf{j}}_{\mathrm{N}}(\mathbf{r},\boldsymbol{\omega}) = -i\boldsymbol{\omega}\hat{\mathbf{P}}_{\mathrm{N}}(\mathbf{r},\boldsymbol{\omega}) + \overrightarrow{\nabla} \times \hat{\mathbf{M}}_{\mathrm{N}}(\mathbf{r},\boldsymbol{\omega}) = (-i\boldsymbol{\omega}, \quad \overrightarrow{\nabla}\times) \cdot \begin{pmatrix} \hat{\mathbf{P}}_{\mathrm{N}}(\mathbf{r},\boldsymbol{\omega}) \\ \hat{\mathbf{M}}_{\mathrm{N}}(\mathbf{r},\boldsymbol{\omega}) \end{pmatrix}. \tag{20}$$

The noise polarization and noise magnetization can be expressed in terms of the creation and annihilation operators for the electric and the magnetic fields $\hat{\mathbf{f}}_{\mathrm{e}}$, $\hat{\mathbf{f}}_{\mathrm{e}}^{\dagger}$, $\hat{\mathbf{f}}_{\mathrm{m}}$, and $\hat{\mathbf{f}}_{\mathrm{m}}^{\dagger}$

$$\begin{pmatrix} \hat{\mathbf{P}}_{\mathrm{N}} \\ \hat{\mathbf{M}}_{\mathrm{N}} \end{pmatrix} = \sqrt{\frac{\hbar}{\pi}}\mathscr{R} \star \begin{pmatrix} \hat{\mathbf{f}}_{\mathrm{e}} \\ \hat{\mathbf{f}}_{\mathrm{m}} \end{pmatrix}. \tag{21}$$

The Green's tensor $\mathbf{G}$ from Eq. (5) solves the respective Helmholtz equation

$$-\mu_0(-i\boldsymbol{\omega}, \quad \overrightarrow{\nabla}\times) \star \mathscr{M} \star \begin{pmatrix} i\boldsymbol{\omega} \\ \overrightarrow{\nabla}\times \end{pmatrix} \star \mathbf{G} = \delta, \tag{22}$$

with the matrix

$$\mathscr{M} = \begin{pmatrix} \varepsilon_0(\boldsymbol{\epsilon} - \boldsymbol{\xi} \star \boldsymbol{\mu}^{-1} \star \boldsymbol{\zeta}) & \frac{\boldsymbol{\xi}\star\boldsymbol{\mu}^{-1}}{Z_0} \\ \frac{\boldsymbol{\mu}^{-1}\star\boldsymbol{\zeta}}{Z_0} & -\frac{\boldsymbol{\mu}^{-1}}{\mu_0} \end{pmatrix}. \tag{23}$$

The Helmholtz equation reduces to the standard form [3] if all cross susceptibilities are set to 0. The tensor $\mathscr{R}$ is related to the matrix $\mathscr{M}$ via

$$\mathscr{R} \star \mathscr{R}^{*T} = \mathcal{I}[\mathscr{M}]. \tag{24}$$

The conductivity matrix $\mathbf{Q}$ can also be expressed in terms of $\mathscr{M}$

$$\mathbf{Q} = \frac{1}{i\boldsymbol{\omega}}(-i\boldsymbol{\omega}, \quad \overrightarrow{\nabla}\times) \star \left[\mathscr{M} - \begin{pmatrix} \varepsilon_0 & 0 \\ 0 & -\frac{1}{\mu_0} \end{pmatrix}\right] \star \begin{pmatrix} i\boldsymbol{\omega} \\ -\times\overleftarrow{\nabla} \end{pmatrix}. \tag{25}$$

Calculations of the equations of motion of the creation and annihilation operators require the field Hamiltonian $\hat{H}_\mathrm{F}$,

$$\hat{H}_\mathrm{F} = \sum_{\lambda=\mathrm{e,m}} \int d^3r \int_0^\infty d\omega \hbar\omega \hat{\mathbf{f}}^\dagger_\lambda(\mathbf{r},\omega)\cdot\hat{\mathbf{f}}_\lambda(\mathbf{r},\omega), \tag{26}$$

and the interaction Hamiltonian $\hat{H}_\mathrm{AF}$ (7). Inserting Eqs. (4), (5), (20), and (21) into Eq. (7) enables us to solve the linear and inhomogeneous differential equation of the field operators

$$\begin{aligned}\begin{pmatrix}\hat{\mathbf{f}}_\mathrm{e}(\mathbf{r},\omega,t)\\ \hat{\mathbf{f}}_\mathrm{m}(\mathbf{r},\omega,t)\end{pmatrix} &= e^{-i\omega(t-t_0)}\begin{pmatrix}\hat{\mathbf{f}}_\mathrm{e}(\mathbf{r},\omega)\\ \hat{\mathbf{f}}_\mathrm{m}(\mathbf{r},\omega)\end{pmatrix} + \frac{\mu_0\omega}{\hbar}\sqrt{\frac{\hbar}{\pi}}\sum_{m,n}\int_0^{t_0} dt'\\ &\times [\mathbf{G}\star(-i\omega,\overrightarrow{\nabla}\times)\star\mathscr{R}]^{*\mathrm{T}}(\mathbf{r}_A,\mathbf{r},\omega)\\ &\times e^{-i\omega(t-t')}\cdot\mathbf{d}_{mn}\hat{A}_{mn},\end{aligned} \tag{27}$$

which can be inserted into Eqs. (21), (20), and (5) again. After using Eqs. (25) and (16) again, the final expression for $\hat{\mathbf{E}}(\mathbf{r},\omega)$ yields

$$\begin{aligned}\hat{\mathbf{E}}(\mathbf{r},\omega,t) &= e^{-i\omega(t-t_0)}\hat{\mathbf{E}}(\mathbf{r},\omega) + i\frac{\mu_0\omega^2}{\pi}\sum_{m,n}\int_{t_0}^{t} dt' e^{-i\omega(t-t')}\\ &\times \mathcal{I}[\mathbf{G}(\mathbf{r},\mathbf{r}_A,\omega)]\cdot\mathbf{d}_{mn}\hat{A}_{mn}\end{aligned} \tag{28}$$

and agrees perfectly with the result from Sec. II A [Eq. (17)].

III. INTERNAL ATOMIC DYNAMICS: FREQUENCY SHIFT AND DECAY RATE

The internal atomic dynamics can be described by the Heisenberg equations of motion for the atomic flip operator

$$\dot{\hat{A}}_{mn} = \frac{1}{i\hbar}[\hat{A}_{mn},\hat{H}] = \frac{1}{i\hbar}[\hat{A}_{mn},\hat{H}_\mathrm{A}] + \frac{1}{i\hbar}[\hat{A}_{mn},\hat{H}_\mathrm{AF}], \tag{29}$$

which includes only the atomic Hamiltonian $\hat{H}_\mathrm{A}$ and the interaction Hamiltonian $\hat{H}_\mathrm{AF}$ because the field Hamiltonian $\hat{H}_\mathrm{F}$ commutes with the atomic flip operator. This approach follows the procedure for a reciprocal surface outlined in Ref. [4] and is now extended to nonreciprocal media [26].

This leads to

$$\begin{aligned}\dot{\hat{A}}_{mn} &= i\omega_{mn}\hat{A}_{mn} + \frac{i}{\hbar}\sum_k\int_0^\infty d\omega\\ &\times [(\hat{A}_{mk}\mathbf{d}_{nk} - \hat{A}_{kn}\mathbf{d}_{km})\cdot\hat{\mathbf{E}}(\mathbf{r}_A,\omega)\\ &+ \hat{\mathbf{E}}^\dagger(\mathbf{r}_A,\omega)\cdot(\mathbf{d}_{nk}\hat{A}_{mk} - \mathbf{d}_{km}\hat{A}_{kn})].\end{aligned} \tag{30}$$

$\hat{A}_{mn}$ is dominated by oscillations with frequencies $\tilde{\omega}_{mn} = \omega_{mn} + \delta\omega_{mn}$, where ω_{mn} is the atom's eigenfrequency and $\delta\omega_{mn}$ is the shift owing to interaction with nearby material bodies (Casimir–Polder shift). The electric field is given in Eqs. (17) or (28). The time integral in the electric field can be formally evaluated in the Markov approximation where we neglect the slow nonoscillatory dynamics of the atomic flip operator $\hat{A}_{mn}$ during the time interval $t_0 \leqslant t' \leqslant t$ and set $\hat{A}_{mn}(t') \simeq \exp[i\tilde{\omega}_{mn}(t'-t)]\hat{A}_{mn}(t)$, where we have anticipated the result $\tilde{\omega}_{mn} = -\tilde{\omega}_{nm}$. In the long-time limit $t\to\infty$ the time integral reduces to $\hat{A}_{mn}(t)\int_{t_0}^t dt' \exp[-i(\omega-\tilde{\omega}_{nm})(t-t')] \simeq \hat{A}_{mn}(t)[\pi\delta(\omega-\tilde{\omega}_{nm}) - i\mathscr{P}/(\omega-\tilde{\omega}_{nm})]$, where $\mathscr{P}$ is the Cauchy principle value and the limits of the frequency integral will lead to the appearance of the Heaviside step-function Θ.

By defining the coefficient

$$\begin{aligned}\mathbf{C}_{mn} &= \frac{\mu_0}{\hbar}\Theta(\tilde{\omega}_{nm})\tilde{\omega}_{nm}^2\mathcal{I}[\mathbf{G}(\mathbf{r}_\mathrm{A},\mathbf{r}_\mathrm{A},\tilde{\omega}_{nm})]\cdot\mathbf{d}_{mn}\\ &- i\frac{\mu_0}{\pi\hbar}\mathscr{P}\int_0^\infty d\omega\frac{1}{\omega-\tilde{\omega}_{nm}}\omega^2\mathcal{I}[\mathbf{G}(\mathbf{r}_\mathrm{A},\mathbf{r}_\mathrm{A},\omega)]\cdot\mathbf{d}_{mn},\end{aligned} \tag{31}$$

Eq. (30) can be cast into the form

$$\begin{aligned}\dot{\hat{A}}_{mn}(t) &= i\omega_{mn}\hat{A}_{nm}(t) + \frac{i}{\hbar}\sum_k\int_0^\infty d\omega\\ &\times \{e^{-i\omega(t-t_0)}[\hat{A}_{mk}(t)\mathbf{d}_{nk} - \hat{A}_{kn}(t)\mathbf{d}_{km}]\cdot\hat{\mathbf{E}}(\mathbf{r}_\mathrm{A},\omega)\\ &+ e^{i\omega(t-t_0)}\hat{\mathbf{E}}^\dagger(\mathbf{r}_\mathrm{A},\omega)\cdot[\mathbf{d}_{nk}\hat{A}_{mk}(t) - \mathbf{d}_{km}\hat{A}_{kn}(t)]\}\\ &- \sum_{k,l}[\mathbf{d}_{nk}\cdot\mathbf{C}_{kl}\hat{A}_{ml}(t) - \mathbf{d}_{km}\cdot\mathbf{C}_{nl}\hat{A}_{kl}(t)]\\ &+ \sum_{k,l}[\mathbf{d}_{nk}\cdot\mathbf{C}^*_{ml}\hat{A}_{lk}(t) - \mathbf{d}_{km}\cdot\mathbf{C}^*_{kl}\hat{A}_{ln}(t)],\end{aligned} \tag{32}$$

where we have used the identity $\mathcal{I}[\mathbf{G}^*(\mathbf{r}_\mathrm{A},\mathbf{r}_\mathrm{A},\omega)] = \mathcal{I}[\mathbf{G}^\mathrm{T}(\mathbf{r}_\mathrm{A},\mathbf{r}_\mathrm{A},\omega)]$, which can be derived from Eq. (3).

Next, we take expectation values of Eq. (32) and assume the electromagnetic field to be prepared in its ground state at initial time t_0 which implies $\hat{\mathbf{E}}(\mathbf{r},\omega)|\{0\}\rangle = \mathbf{0}$. Therefore, the free terms of the electric field $\hat{\mathbf{E}}(\mathbf{r},\omega)$ and $\hat{\mathbf{E}}^\dagger(\mathbf{r},\omega)$ do not contribute to the dynamics of the average value of the atomic flip operator and are discarded.

Since we assume the atom to be free of quasidegenerate transitions, the set of differential equations for the atomic flip operator's expectation value can be decoupled. Moreover, the atom is unpolarized in each of its energy eigenstates, $\hat{\mathbf{d}}_{nn} = 0$, which is guaranteed by atomic selection rules [4]. As a result of these assumptions, the fast-oscillating off-diagonal flip operators decouple from the nonoscillating diagonal ones as well as from each other [4].

By making use of Eq. (3) we find that the two terms $\mathbf{d}_{nk}\cdot\mathcal{I}[\mathbf{G}(\mathbf{r}_A,\mathbf{r}_A,\omega)]\cdot\mathbf{d}_{kn} = \mathcal{I}[\mathbf{d}_{nk}\cdot\mathbf{G}(\mathbf{r}_A,\mathbf{r}_A,\omega)\cdot\mathbf{d}_{kn}]$ and $\mathbf{d}_{kn}\cdot\mathcal{I}[\mathbf{G}^\mathrm{T}(\mathbf{r}_A,\mathbf{r}_A,\omega)]\cdot\mathbf{d}_{nk} = \mathcal{I}[\mathbf{d}_{nk}\cdot\mathbf{G}(\mathbf{r}_A,\mathbf{r}_A,\omega)\cdot\mathbf{d}_{kn}]$ are equal and real.

With the help of these relations we identify the decay rate

$$\Gamma_{nk} = \frac{2\mu_0}{\hbar}\tilde{\omega}_{nk}^2\mathcal{I}[\mathbf{d}_{nk}\cdot\mathbf{G}(\mathbf{r}_A,\mathbf{r}_A,\tilde{\omega}_{nk})\cdot\mathbf{d}_{kn}] \tag{33}$$

and the frequency shift

$$\begin{aligned}\delta\omega_{nk} &= -\frac{\mu_0}{\pi\hbar}\mathscr{P}\int_0^\infty d\omega\frac{1}{\omega-\tilde{\omega}_{nk}}\omega^2\\ &\times\mathcal{I}[\mathbf{d}_{nk}\cdot\mathbf{G}^{(1)}(\mathbf{r}_A,\mathbf{r}_A,\omega)\cdot\mathbf{d}_{kn}].\end{aligned} \tag{34}$$

Here, the Green's tensor $\mathbf{G}$ has been split into a bulk part $\mathbf{G}^{(0)}$ and a scattering part $\mathbf{G}^{(1)}$. The Lamb shift due to the free-space Green's tensor $\mathbf{G}^{(0)}$ is already included in the transition frequency ω_{mn}, which refers solely to the atom and does not take the material properties of surrounding matter into account. The remaining frequency shift stems from the presence of electromagnetic bodies around the atom.

Finally, the expectation value for the atomic flip operator for the nondiagonal terms yields

$$\langle\dot{\hat{A}}_{mn}(t)\rangle = i\boldsymbol{\omega}_{mn}\langle\hat{A}_{mn}(t)\rangle + \sum_k\left(-\frac{1}{2}\Gamma_{nk} - i\delta\boldsymbol{\omega}_{nk}\right)\langle\hat{A}_{mn}(t)\rangle + \sum_k\left(-\frac{1}{2}\Gamma_{mk} + i\delta\boldsymbol{\omega}_{mk}\right)\langle\hat{A}_{mn}(t)\rangle. \quad (35)$$

We define $\delta\boldsymbol{\omega}_n = \sum_k \delta\boldsymbol{\omega}_{nk}$ and $\Gamma_n = \sum_{k<n}\Gamma_{nk}$—the Θ function in Eq. (31) determines the order of summation indices—and the shifted transition frequency as

$$\tilde{\boldsymbol{\omega}}_{mn} = \boldsymbol{\omega}_{mn} + \delta\boldsymbol{\omega}_m - \delta\boldsymbol{\omega}_n, \quad (36)$$

which verifies our previous assumption $\tilde{\boldsymbol{\omega}}_{mn} = -\tilde{\boldsymbol{\omega}}_{nm}$. Thus Eq. (32) for the diagonal terms has the simple form

$$\langle\dot{\hat{A}}_{nn}(t)\rangle = -\Gamma_n\langle\hat{A}_{nn}(t)\rangle + \sum_{k>n}\Gamma_{kn}\langle\hat{A}_{kk}(t)\rangle. \quad (37)$$

Since the shifted frequency $\tilde{\boldsymbol{\omega}}_{nk}$ appears in $\delta\boldsymbol{\omega}_{nk}$ itself, the frequency shift is given as a self-consistent result from the implicit equation.

The frequency shift (34) can be simplified further by making use of the definition of the imaginary part (3), the Schwarz principle which is still valid for nonreciprocal media,

$$\mathbf{G}^*(\mathbf{r}_A,\mathbf{r}_A,\boldsymbol{\omega}) = \mathbf{G}(\mathbf{r}_A,\mathbf{r}_A,-\boldsymbol{\omega}^*), \quad (38)$$

and a substitution $\boldsymbol{\omega}\to-\boldsymbol{\omega}$ in the second integral having its origin in Eq. (3). The integral contours along the positive and negative real axes have one pole each and are evaluated in the complex plane. The path along the quarter circle does not give a contribution because $\lim_{|\boldsymbol{\omega}|\to0}\mathbf{G}^{(1)}(\mathbf{r},\mathbf{r}',\boldsymbol{\omega})\boldsymbol{\omega}^2/c^2 = 0$. The part along the imaginary axis leads to the nonresonant frequency shift

$$\delta\boldsymbol{\omega}_{nk}^{\mathrm{nres}} = \frac{\mu_0}{\pi\hbar}\int_0^\infty d\xi\,\frac{\xi^3}{\xi^2+\tilde{\boldsymbol{\omega}}_{nk}^2}\mathcal{I}[\mathbf{d}_{nk}\cdot\mathbf{G}^{(1)}(\mathbf{r}_A,\mathbf{r}_A,i\xi)\cdot\mathbf{d}_{kn}] - \frac{\mu_0}{\pi\hbar}\int_0^\infty d\xi\,\frac{\xi^2\tilde{\boldsymbol{\omega}}_{nk}}{\xi^2+\tilde{\boldsymbol{\omega}}_{nk}^2} \times\mathcal{R}[\mathbf{d}_{nk}\cdot\mathbf{G}^{(1)}(\mathbf{r}_A,\mathbf{r}_A,i\xi)\cdot\mathbf{d}_{kn}], \quad (39)$$

with a Green's function $\mathbf{G}$ with imaginary frequency $\boldsymbol{\omega}\to i\xi$. This expression resembles the frequency shift of the Casimir–Polder force for an atom in its ground state [3]. It comes from the exchange of virtual photons between the atom and the material body. This entirely quantum-mechanical interpretation can be extended for an atom in an arbitrary state. The matrix-vector product of the Green's tensor and the dipole moments is real for a reciprocal medium and therefore only the second contribution remains in this case.

The evaluation of the poles gives the resonant contribution associated with real-photon emission and a real-frequency expression $\tilde{\boldsymbol{\omega}}_{nk}$

$$\delta\boldsymbol{\omega}_{nk}^{\mathrm{res}} = -\frac{\mu_0}{\hbar}\tilde{\boldsymbol{\omega}}_{nk}^2\mathcal{R}[\mathbf{d}_{nk}\cdot\mathbf{G}^{(1)}(\mathbf{r}_A,\mathbf{r}_A,\tilde{\boldsymbol{\omega}}_{nk})\cdot\mathbf{d}_{kn}]. \quad (40)$$

In case of the resonant frequency shift, the Green's tensor $\mathbf{G}$ in Eq. (40) contains discrete frequencies for the real atomic transitions to a lower energy state, which can only occur for excited atoms and is related to real exchange photons.

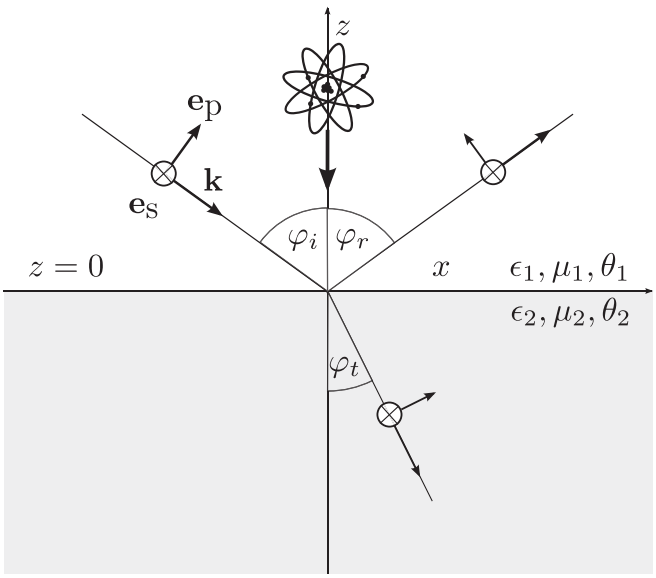

FIG. 1. Sketch of an atom in front of a medium with electric and magnetic properties and an axion coupling. The direction of incoming parallely polarized light $\mathbf{e}_\mathrm{p}$ and perpendicularly polarized light $\mathbf{e}_\mathrm{s}$ are shown.

The sum of the resonant and nonresonant frequency shifts $\delta\boldsymbol{\omega}_{nk}$ over all indices k can be identified with the total position-dependent Casimir–Polder potential. Its derivative with respect to position is the Casimir–Polder force between the atom and the nonreciprocal medium, which is caused by the atom's level-shift due to the body's presence.

IV. APPLICATIONS AND RESULTS

Having derived expressions for the atomic rate of spontaneous decay (33) and nonresonant and resonant frequency shifts [Eqs. (39) and (40)], we contrast a perfectly reflecting nonreciprocal mirror with a perfectly conducting mirror. Afterward we compare this to a topological insulator from Ref. [46]. Figure 1 shows a sketch of an atom in front of a medium having electric, magnetic properties and an axion coupling. The scattering part of the Green's tensor $\mathbf{G}^{(1)}$ of a single planar surface has the form [46]

$$\mathbf{G}^{(1)}(\mathbf{r},\mathbf{r}',\boldsymbol{\omega}) = \frac{i}{8\pi^2}\int d^2k^{\parallel}\frac{1}{k^{\perp}}\sum_{\sigma=\mathrm{s,p}}\sum_{\sigma'=\mathrm{s,p}} r_{\sigma,\sigma'} \times\mathbf{e}_{\sigma+}\mathbf{e}_{\sigma'-}e^{i\mathbf{k}^{\parallel}(\mathbf{r}-\mathbf{r}')}e^{ik^{\perp}(z+z')}, \quad (41)$$

with the two unit vectors $\mathbf{e}_{\sigma+}$ and $\mathbf{e}_{\sigma'-}$ representing the polarizations of incident (σ') and reflected waves (σ). The reflective coefficient $r_{\sigma,\sigma'}$ takes the mixing of the incoming and outgoing polarizations σ' and σ into account. The indices p and s refer to parallel or perpendicular polarization, respectively. $\mathbf{k}^{\parallel}$ represents the parallel component of the wave vector, $\mathbf{k}^{\perp}$ is its perpendicular component, and z is the vertical distance to the surface.

According to Curie's principle a system consisting of a crystal and an external influence, each having a specific symmetry, only maintains the symmetries that are shared by both the crystal and the external influence [47]. Hence our choice of

dipole moments must be such that the atom is sensitive to the violated time-reversal symmetry of a perfectly reflecting nonreciprocal mirror. To study possible effects of nonreciprocity, we assume circularly polarized dipole moments

$$\mathbf{d}_{10} = \frac{d}{\sqrt{2}}\begin{pmatrix}1\\ i\\ 0\end{pmatrix}, \quad \mathbf{d}_{01} = \frac{d}{\sqrt{2}}\begin{pmatrix}1\\ -i\\ 0\end{pmatrix}, \tag{42}$$

which are not invariant if the direction of time is reversed $t \to -t$.

A. Perfectly conducting mirror

Let us first investigate the atomic decay rate (33) and the nonresonant and resonant frequency shift (39), (40) for a perfectly conducting mirror. The energy shift of a hydrogen atom between two conducting plates has been studied in Refs. [48,49] and one can obtain the interaction between an atom and a single plate if one plate is shifted to infinity. Reference [50] shows the radiative decay rate of an atom in front of a perfect mirror, where the dipole is either parallel or perpendicular to the mirror. These approaches are based on perturbation theory.

The reflective coefficients for a perfectly conducting mirror are $r_{\mathrm{p,p}} = 1$, $r_{\mathrm{s,s}} = -1$, and $r_{\mathrm{s,p}} = r_{\mathrm{p,s}} = 0$. This set of coefficients is obtained from the reflective coefficients for a general material in the limit $\varepsilon \to \infty$, which is explained in greater detail in Sec. IV C. In this case the Green's tensor (41) contains only diagonal terms with $\mathbf{G}^{(1)}_{xx} = \mathbf{G}^{(1)}_{yy}$

$$\mathbf{G}^{(1)}_{xx}(\mathbf{r},\mathbf{r},\boldsymbol{\omega}) = \left(-\frac{1}{8\pi z} - i\frac{c}{16\pi\boldsymbol{\omega}z^2} + \frac{c^2}{32\pi\boldsymbol{\omega}^2 z^3}\right)e^{\frac{2i\boldsymbol{\omega}z}{c}}. \tag{43}$$

The nondiagonal elements of the Green's tensor vanish. The atomic decay rate (33) for circularly polarized dipole moments (42) hence reads

$$\Gamma^{(1)}_{10} = \frac{\mu_0\tilde{\boldsymbol{\omega}}^2_{10}d^2}{4\pi\hbar}\left[-\frac{1}{z}\sin\left(\frac{2\tilde{\boldsymbol{\omega}}_{10}z}{c}\right) - \frac{c}{2\tilde{\boldsymbol{\omega}}_{10}z^2}\cos\left(\frac{2\tilde{\boldsymbol{\omega}}_{10}z}{c}\right) + \frac{c^2}{4\tilde{\boldsymbol{\omega}}^2_{10}z^3}\sin\left(\frac{2\tilde{\boldsymbol{\omega}}_{10}z}{c}\right)\right]. \tag{44}$$

Figure 2 shows the atomic decay rate (44) scaled by the free-space decay rate

$$\Gamma^{(0)}_{10} = \frac{\mu_0\tilde{\boldsymbol{\omega}}^3_{10}d^2}{3\pi\hbar c}. \tag{45}$$

Moreover we study the asymptotic behavior of the decay rate and distinguish between the retarded limit ($\tilde{\boldsymbol{\omega}}_{10}z/c \gg 1$) and the nonretarded limit ($\tilde{\boldsymbol{\omega}}_{10}z/c \ll 1$). The decay rate decays asymptotically in the retarded limit with $-[\mu_0\tilde{\boldsymbol{\omega}}^2_{10}d^2\sin(2\tilde{\boldsymbol{\omega}}_{10}z/c)]/[4\pi\hbar z]$.

At $z = 0$, in the nonretarded limit, the decay rate has a value of $-\Gamma^{(0)}_{10}$ (Fig. 2). The total decay rate Γ_{10} of a dipole parallel to a perfectly conducting mirror is a sum of the free-space part $\Gamma^{(0)}_{10}$ and the body-induced part $\Gamma^{(1)}_{10}$ and is equal to $\Gamma_{10} = \Gamma^{(0)}_{10} + \Gamma^{(1)}_{10} = 0$ on the surface of the mirror at $z = 0$. This can be explained by an image dipole with equal strength and opposite direction induced by the original one so that the two dipoles cancel, leading to vanishing radiative decay.

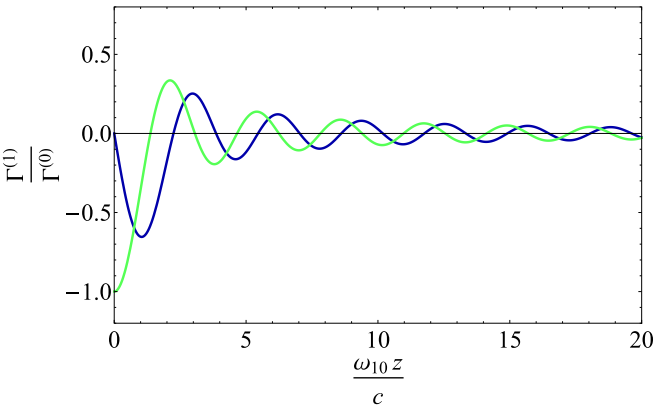

FIG. 2. Atomic decay rates $\Gamma^{(1)}$ scaled by the free-space decay rate $\Gamma^{(0)}$ (45) for a circularly polarized two-level atomic dipole in front of a perfectly conducting mirror (green line) and a perfectly reflecting nonreciprocal mirror (blue line).

The frequency shift is composed of a resonant and a nonresonant contribution

$$\begin{aligned}\delta\boldsymbol{\omega}_{10} &= \delta\boldsymbol{\omega}^{\mathrm{res}}_{10} + \delta\boldsymbol{\omega}^{\mathrm{nres}}_{10}\\ &= \frac{\mu_0\tilde{\boldsymbol{\omega}}^2_{10}d^2}{8\pi\hbar}\left[\frac{1}{z}\cos\left(\frac{2\tilde{\boldsymbol{\omega}}_{10}z}{c}\right) - \frac{c}{2\tilde{\boldsymbol{\omega}}_{10}z^2}\sin\left(\frac{2\tilde{\boldsymbol{\omega}}_{10}z}{c}\right) - \frac{c^2}{4\tilde{\boldsymbol{\omega}}^2_{10}z^3}\cos\left(\frac{2\tilde{\boldsymbol{\omega}}_{10}z}{c}\right)\right]\\ &\quad + \frac{\mu_0 d^2}{8\pi^2\hbar}\int_0^\infty d\xi\,\frac{\tilde{\boldsymbol{\omega}}_{10}\xi^2}{\tilde{\boldsymbol{\omega}}^2_{10}+\xi^2}\left(\frac{1}{z} + \frac{c}{2\xi z^2} + \frac{c^2}{4\xi^2 z^3}\right)e^{-\frac{2\xi z}{c}},\end{aligned} \tag{46}$$

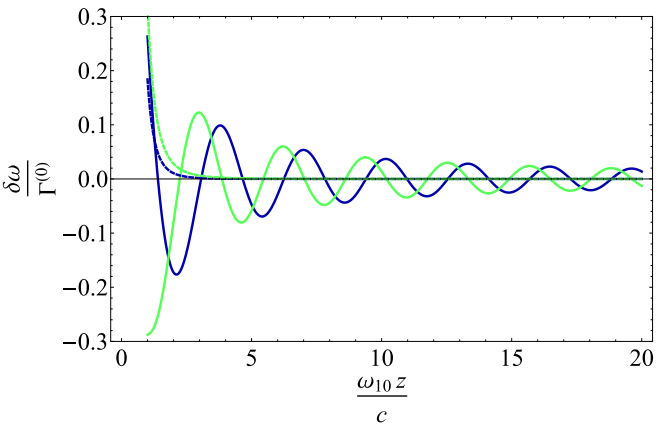

FIG. 3. Frequency shifts $\delta\boldsymbol{\omega}$ scaled by the free-space decay rate $\Gamma^{(0)}$ (45) for a circularly polarized two-level atomic dipole in front of a perfectly reflecting nonreciprocal mirror and a perfectly conducting mirror. The resonant frequency shift $\delta\boldsymbol{\omega}^{\mathrm{res}}$ of the perfectly conducting mirror (green line) and the resonant frequency shift of the perfectly reflecting nonreciprocal mirror (blue line) show oscillations. The nonresonant frequency shift $\delta\boldsymbol{\omega}^{\mathrm{nres}}$ of the perfectly conducting mirror (dashed green line) and the perfectly reflecting nonreciprocal mirror (dashed blue line) decay monotonically with distance.

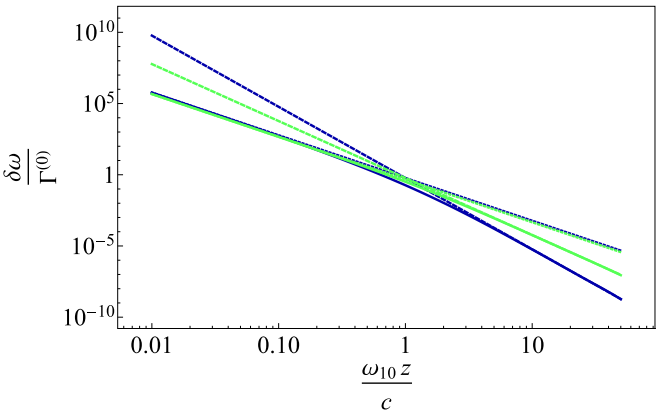

FIG. 4. Double-logarithmic plot for the nonresonant frequency shift $\delta\boldsymbol{\omega}^{\mathrm{nres}}$ of the perfectly conducting mirror (green line), its retarded limit (green dashed line), and its nonretarded limit (green dotted line). The perfectly reflecting nonreciprocal mirror (blue line), its retarded limit (blue dashed line), and its nonretarded limit (blue dotted line) are depicted in the same figure.

which are shown in Fig. 3. The retarded and nonretarded limits of the nonresonant frequency shift (46) read

$$\delta\boldsymbol{\omega}_{10}^{\mathrm{nres}} = \begin{cases} \dfrac{d^2 c}{16\pi^2\varepsilon_0\hbar\tilde{\boldsymbol{\omega}}_{10} z^4}, & \dfrac{\tilde{\boldsymbol{\omega}}_{10} z}{c} \gg 1 \\ \dfrac{d^2}{64\pi\varepsilon_0\hbar z^3}, & \dfrac{\tilde{\boldsymbol{\omega}}_{10} z}{c} \ll 1, \end{cases} \tag{47}$$

and are depicted in a double-logarithmic plot in Fig. 4. The asymptotic limits of the resonant frequency shift (46) read

$$\delta\boldsymbol{\omega}_{10}^{\mathrm{res}} = \begin{cases} \dfrac{\mu_0\tilde{\boldsymbol{\omega}}_{10}^2 d^2}{8\pi\hbar z}\cos\left(\dfrac{2\tilde{\boldsymbol{\omega}}_{10} z}{c}\right), & \dfrac{\tilde{\boldsymbol{\omega}}_{10} z}{c} \gg 1 \\ -\dfrac{d^2}{32\pi\varepsilon_0\hbar z^3}, & \dfrac{\tilde{\boldsymbol{\omega}}_{10} z}{c} \ll 1 \end{cases} \tag{48}$$

and are shown in Fig. 3 as well.

B. Perfectly reflecting nonreciprocal mirror

The reflection coefficients for incoming perpendicular or parallel polarization and outgoing perpendicular or parallel polarization $r_{\mathrm{s,s}}$ and $r_{\mathrm{p,p}}$ are set equal to 0, whereas the mixing terms $r_{\mathrm{s,p}}$ and $r_{\mathrm{p,s}}$ can be chosen to be either 1 or -1 thus generating a perfectly reflecting nonreciprocal mirror. In this section, we restrict ourselves to the case $r_{\mathrm{s,p}} = r_{\mathrm{p,s}} = -1$. These reflective coefficients are the specific case of a perfect electromagnetic conductor (PEMC) with parameter $M = 1$ [51–53], which is explained in Sec. IV C. The Green's tensor (41) is antisymmetric under these conditions: $\mathbf{G}^{(1)\mathrm{T}}(\mathbf{r},\mathbf{r}',\boldsymbol{\omega}) = -\mathbf{G}^{(1)}(\mathbf{r}',\mathbf{r},\boldsymbol{\omega})$. Thus the diagonal terms of the Green's tensor vanish and only the nondiagonal terms remain. By interchanging the indices of the nondiagonal terms, $\mathbf{G}_{xz}^{(1)}(\mathbf{r},\mathbf{r}') = \mathbf{G}_{zx}^{(1)}(\mathbf{r},\mathbf{r}')$ and $\mathbf{G}_{yz}^{(1)}(\mathbf{r},\mathbf{r}') = \mathbf{G}_{zy}^{(1)}(\mathbf{r},\mathbf{r}')$ keep their signs, whereas $\mathbf{G}_{xy}^{(1)}(\mathbf{r},\mathbf{r}') = -\mathbf{G}_{yx}^{(1)}(\mathbf{r},\mathbf{r}')$ shows a sign change. This behavior is exactly opposite if the arguments of the nondiagonal terms are interchanged. Therefore $\mathbf{G}_{xz}^{(1)}$ and $\mathbf{G}_{yz}^{(1)}$ have to vanish by setting $\mathbf{r} = \mathbf{r}'$ and only $\mathbf{G}_{xy}^{(1)} = -\mathbf{G}_{yx}^{(1)}$ has finite values. The final result after integrating yields

$$\mathbf{G}_{xy}^{(1)}(\mathbf{r},\mathbf{r},\boldsymbol{\omega}) = \left(-\frac{1}{8\pi z} - i\frac{c}{16\pi\boldsymbol{\omega} z^2}\right)e^{\frac{2i\boldsymbol{\omega} z}{c}}. \tag{49}$$

By using the circularly polarized dipole moments (42), we obtain for the atomic decay rate

$$\Gamma_{10}^{(1)} = \frac{\mu_0\tilde{\boldsymbol{\omega}}_{10}^2 d^2}{4\pi\hbar}\left[\frac{1}{z}\cos\left(\frac{2\tilde{\boldsymbol{\omega}}_{10} z}{c}\right) - \frac{c}{2\tilde{\boldsymbol{\omega}}_{10} z^2}\sin\left(\frac{2\tilde{\boldsymbol{\omega}}_{10} z}{c}\right)\right], \tag{50}$$

which is shown in Fig. 2. The decay rate of a perfectly reflecting nonreciprocal mirror is equal to zero for small values of $\tilde{\boldsymbol{\omega}}_{10} z/c$ (nonretarded limit). The function decays asymptotically in the retarded limit with $[\mu_0\tilde{\boldsymbol{\omega}}_{10}^2 d^2\cos(2\tilde{\boldsymbol{\omega}}_{10} z/c)]/[4\pi\hbar z]$.

The frequency shift is shown in Fig. 3 and consists of a resonant and a nonresonant contribution

$$\begin{aligned}\delta\boldsymbol{\omega}_{10} &= \delta\boldsymbol{\omega}_{10}^{\mathrm{res}} + \delta\boldsymbol{\omega}_{10}^{\mathrm{nres}} \\ &= \frac{\mu_0\tilde{\boldsymbol{\omega}}_{10}^2 d^2}{8\pi\hbar}\left[\frac{1}{z}\sin\left(\frac{2\tilde{\boldsymbol{\omega}}_{10} z}{c}\right) + \frac{c}{2\tilde{\boldsymbol{\omega}}_{10} z^2}\cos\left(\frac{2\tilde{\boldsymbol{\omega}}_{10} z}{c}\right)\right] \\ &\quad + \frac{\mu_0 d^2}{8\pi^2\hbar}\int_0^\infty d\xi\,\frac{\xi^3}{\xi^2 + \tilde{\boldsymbol{\omega}}_{10}^2}\left(\frac{1}{z} + \frac{c}{2\xi z^2}\right)e^{-\frac{2\xi z}{c}}.\end{aligned} \tag{51}$$

In the retarded and nonretarded limits the nonresonant part has the asymptotic behavior,

$$\delta\boldsymbol{\omega}_{10}^{\mathrm{nres}} = \begin{cases} \dfrac{d^2 c^2}{16\pi^2\varepsilon_0\hbar\tilde{\boldsymbol{\omega}}_{10}^2 z^5}, & \dfrac{\tilde{\boldsymbol{\omega}}_{10} z}{c} \gg 1 \\ \dfrac{d^2}{16\pi^2\varepsilon_0\hbar z^3}, & \dfrac{\tilde{\boldsymbol{\omega}}_{10} z}{c} \ll 1, \end{cases} \tag{52}$$

which is shown in a double-logarithmic plot in Fig. 4. The resonant part has the limits

$$\delta\boldsymbol{\omega}_{10}^{\mathrm{res}} = \begin{cases} \dfrac{\mu_0\tilde{\boldsymbol{\omega}}_{10}^2 d^2}{8\pi\hbar z}\sin\left(\dfrac{2\tilde{\boldsymbol{\omega}}_{10} z}{c}\right), & \dfrac{\tilde{\boldsymbol{\omega}}_{10} z}{c} \gg 1 \\ \dfrac{\mu_0\tilde{\boldsymbol{\omega}}_{10} d^2 c}{16\pi\hbar z^2}, & \dfrac{\tilde{\boldsymbol{\omega}}_{10} z}{c} \ll 1. \end{cases} \tag{53}$$

By comparing both the decay rates and the resonant frequency shifts in Figs. 2 and 3, a phase shift by $\pi/2$ between the respective curves of the perfectly conducting mirror and the perfectly reflecting nonreciprocal mirror is apparent, as can also be read off from the first terms in Eqs. (44), (46), (50), and (51). This is the additional phase shift implied by the reflection of s- into p-polarized waves. The scaling behavior of the decay rates and the resonant frequency shifts in the retarded limit is the same. The decay of the resonant frequency shift in the nonretarded limit is proportional to z^{-3} for the perfectly conducting mirror and z^{-2} for the perfectly reflecting nonreciprocal mirror. As for the nonresonant frequency shift (46) and (51), the perfectly reflecting nonreciprocal mirror decays with z^{-5} in contrast to z^{-4} for the perfectly conducting mirror in the retarded limit. The scaling behavior in the nonretarded limit is z^{-3} for both media.

The term z^{-1} of the total frequency shift, the sum of the resonant and the nonresonant part, will dominate in the retarded limit both for the perfectly conducting mirror and

the perfectly reflecting nonreciprocal mirror. As for the total frequency shift in the nonretarded limit, there is a dominant z^{-3} scaling behavior for both ideal materials.

C. Topological insulator

Reference [46] studies the electromagnetic behavior of a topological insulator. Permittivity, permeability, and the magneto-electric cross susceptibilities for this material mentioned in Eq. (23) are assigned according to

$$\boldsymbol{\epsilon} - \boldsymbol{\xi} \star \boldsymbol{\mu}^{-1} \star \boldsymbol{\zeta} \to \epsilon, \quad \boldsymbol{\xi} \star \boldsymbol{\mu}^{-1} \to \frac{\alpha}{\pi}\theta(\mathbf{r},\boldsymbol{\omega}),$$
$$\boldsymbol{\mu}^{-1} \star \boldsymbol{\zeta} \to \frac{\alpha}{\pi}\theta(\mathbf{r},\boldsymbol{\omega}), \quad \boldsymbol{\mu}^{-1} \to \mu^{-1}, \tag{54}$$

so that Eq. (19) takes the form

$$\hat{\mathbf{D}} = \varepsilon_0\varepsilon\hat{\mathbf{E}} + \frac{\alpha}{\pi}\frac{\theta(\mathbf{r},\boldsymbol{\omega})}{\mu_0 c}\hat{\mathbf{B}} + \hat{\mathbf{P}}_{\mathrm{N}}, \tag{55}$$

$$\hat{\mathbf{H}} = -\frac{\alpha}{\pi}\frac{\theta(\mathbf{r},\boldsymbol{\omega})}{\mu_0 c}\hat{\mathbf{E}} + \frac{1}{\mu_0\mu}\hat{\mathbf{B}} - \hat{\mathbf{M}}_{\mathrm{N}}. \tag{56}$$

Reflective coefficients $r_{\sigma,\sigma'}$ mentioned in Eq. (41) for bi-isotropic media are shown in Ref. [54] and are applied to the specific case of a topological insulator with time-reversal-breaking symmetry in Ref. [46] by making use of the relations in Eq. (54)

$$r_{\mathrm{s,s}} = \frac{(\mu k_1^\perp - k_2^\perp)\mu(\varepsilon k_1^\perp + k_2^\perp) - k_1^\perp k_2^\perp \Delta^2}{(\mu k_1^\perp + k_2^\perp)\mu(\varepsilon k_1^\perp + k_2^\perp) + k_1^\perp k_2^\perp \Delta^2},$$
$$r_{\mathrm{p,s}} = \frac{2k_1^\perp k_2^\perp \mu\Delta}{(\mu k_1^\perp + k_2^\perp)\mu(\varepsilon k_1^\perp + k_2^\perp) + k_1^\perp k_2^\perp \Delta^2},$$
$$r_{\mathrm{p,p}} = \frac{(\mu k_1^\perp + k_2^\perp)\mu(\varepsilon k_1^\perp - k_2^\perp) + k_1^\perp k_2^\perp \Delta^2}{(\mu k_1^\perp + k_2^\perp)\mu(\varepsilon k_1^\perp + k_2^\perp) + k_1^\perp k_2^\perp \Delta^2},$$
$$r_{\mathrm{s,p}} = \frac{2k_1^\perp k_2^\perp \mu\Delta}{(\mu k_1^\perp + k_2^\perp)\mu(\varepsilon k_1^\perp + k_2^\perp) + k_1^\perp k_2^\perp \Delta^2}. \tag{57}$$

In these equations, $k_1^\perp$ and $k_2^\perp$ refer to the perpendicular part of the wave vector in medium 1 and 2 and Δ is given by

$$\Delta = \alpha\frac{1}{\pi}(\theta_2 - \theta_1), \tag{58}$$

where α represents the fine-structure constant and θ_1 and θ_2 are the axion coupling constants in the two media. The first medium is assumed to be vacuum ($\mu_1 = \varepsilon_1 = 1, \theta_1 = 0$) and only the second medium has specific electromagnetic properties μ, ε, and θ.

The reflective coefficients (57) reduce to the respective ones for the perfectly conducting mirror in Sec. IV A by setting the axion coupling to $\Delta = 0$ and the other parameters to $\mu_1 = \mu_2 = 1$ and $\varepsilon_1 = 1$. In the limit $\varepsilon_2 \to \infty$, the reflective coefficients for a perfect electrical conductor ($r_{\mathrm{p,p}} = 1$, $r_{\mathrm{s,s}} = -1$, and $r_{\mathrm{s,p}} = r_{\mathrm{p,s}} = 0$) are obtained.

The reflective coefficients of the perfectly reflecting nonreciprocal mirror from Sec. IV B can also be generated from Eq. (57) with the help of Eq. (54). Medium 1 is treated as vacuum and in medium 2 the cross susceptibilities $\boldsymbol{\zeta}$ and $\boldsymbol{\xi}$ are treated as scalars and are set equal to each other, $\zeta = \xi$. The boundary conditions for the perfect electromagnetic conductor

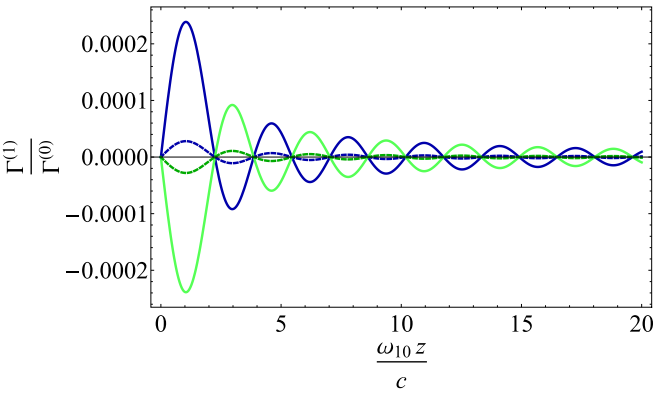

FIG. 5. Atomic decay rates $\Gamma^{(1)}$ for a circularly polarized two-level atomic dipole in front of a topological insulator with $\theta = \pi$ (45) (green line) and $\theta = -\pi$ (blue line) and $\varepsilon = \mu = 1$ scaled by the free-space decay rate $\Gamma^{(0)}$. The difference between the decay rate for Bi_2Se_3 with axion contribution ($\varepsilon = 16$, $\mu = 1$) and the respective decay rate without axion contribution is depicted for an axion coupling of $\theta = \pi$ (green dotted line) and $\theta = -\pi$ (blue dotted line).

(PEMC) read [51–53]

$$\mathbf{n}\cdot\left[\sqrt{\frac{\mu_0}{\varepsilon_0}}\hat{\mathbf{D}} - M\hat{\mathbf{B}}\right] = 0,$$
$$\mathbf{n}\times\left[M\hat{\mathbf{E}} + \sqrt{\frac{\mu_0}{\varepsilon_0}}\hat{\mathbf{H}}\right] = 0, \tag{59}$$

where we have introduced the PEMC parameter $M = \xi/\mu$ and $\mathbf{n}$ represents a unit vector perpendicular to the interface. These conditions imply reflection coefficients

$$r_{\mathrm{s,s}} = \frac{1 - M^2}{1 + M^2}, \quad r_{\mathrm{p,s}} = r_{\mathrm{s,p}} = \frac{-2M}{1 + M^2}, \quad r_{\mathrm{p,p}} = \frac{M^2 - 1}{1 + M^2}, \tag{60}$$

showing that the perfectly reflecting nonreciprocal mirror ($r_{\mathrm{s,s}} = r_{\mathrm{p,p}} = 0$ and $r_{\mathrm{s,p}} = r_{\mathrm{p,s}} = -1$) is a PEMC with parameter $M = 1$. The general PEMC reflection coefficients are recovered from Eq. (57) with Eq. (54) in the limit $\varepsilon, \mu, \xi \to \infty$ while imposing the PEMC condition $\xi^2 - \varepsilon\mu = 0$.

In Ref. [55], the rate of spontaneous decay for an atom close to a topological insulator with axion coupling is also considered. In that work, a linear dipole transition is chosen which is perpendicular or parallel to the surface. In this case, the general expression for the decay rate, unlike Eq. (33), is identical to that for reciprocal material without making use of the definition of the imaginary part of the Green's tensor (3). As a result, the phenomenon is insensitive to the specific time-reversal-symmetry-breaking properties of the topological insulator, as explained above.

Due to the small value of the fine-structure constant α and the small effect on the reflection coefficients (57), we first study a purely axion medium by setting $\varepsilon = 1$ and $\mu = 1$. Figure 5 shows the atomic decay rate for $\theta = \pi$ and $\theta = -\pi$. Figure 6 depicts the respective resonant part of the frequency shift. The results for the decay rate and the resonant frequency shift resemble the respective curves of the perfectly reflecting nonreciprocal mirror in Figs. 2 and 3, but are scaled by $\Delta/2$. This ratio can be easily read off in the retarded and nonretarded

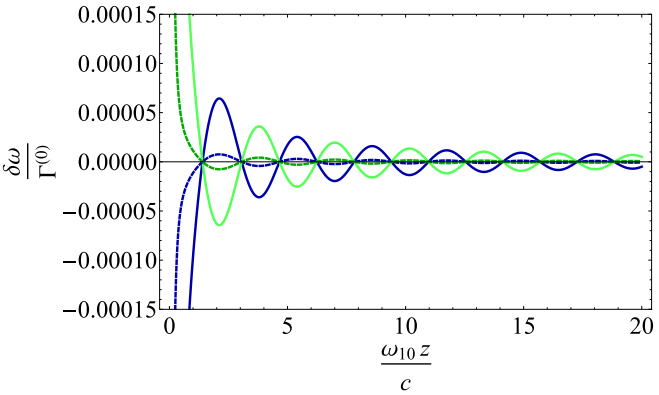

FIG. 6. Resonant frequency shift $\delta\boldsymbol{\omega}^{\mathrm{res}}$ for a circularly polarized two-level atomic dipole in front of a topological insulator (45) with $\theta=\pi$ (green line) and $\theta=-\pi$ (blue line) and $\varepsilon=\mu=1$ scaled by the free-space decay rate $\Gamma^{(0)}$. The difference between the resonant frequency shift for Bi_2Se_3 with axion contribution ($\varepsilon=16$, $\mu=1$) and the respective frequency shift without axion contribution is depicted for an axion coupling of $\theta=\pi$ (green dotted line) and $\theta=-\pi$ (blue dotted line).

limits. The reflective coefficients (57) in the retarded limit read

$$\begin{aligned}
r_{\mathrm{s,s}}^{\mathrm{ret}} &= \frac{(1-\varepsilon)-\Delta^2}{(1+n)^2+\Delta^2},\\
r_{\mathrm{p,s}}^{\mathrm{ret}} &= \frac{-2\Delta}{(1+n)^2+\Delta^2},\\
r_{\mathrm{p,p}}^{\mathrm{ret}} &= \frac{-(1-\varepsilon)+\Delta^2}{(1+n)^2+\Delta^2} = -r_{\mathrm{s,s}}^{\mathrm{ret}},\\
r_{\mathrm{s,p}}^{\mathrm{ret}} &= \frac{-2\Delta}{(1+n)^2+\Delta^2} = r_{\mathrm{p,s}}^{\mathrm{ret}},
\end{aligned} \tag{61}$$

with the refractive index $n=\sqrt{\varepsilon}$. The decay rate and resonant frequency shift with the purely axion contribution in the retarded limit are given by

$$\begin{aligned}
\Gamma_{10}^{(1)\mathrm{ret}}(\varepsilon=1,\theta=\pi) &= \frac{\mu_0\tilde{\boldsymbol{\omega}}_{10}^2 d^2}{4\pi\hbar z}\cos\left(\frac{2\tilde{\boldsymbol{\omega}}_{10}z}{c}\right)\frac{\Delta}{2},\\
\delta\boldsymbol{\omega}_{10}^{\mathrm{res,ret}}(\varepsilon=1,\theta=\pi) &= \frac{\mu_0\tilde{\boldsymbol{\omega}}_{10}^2 d^2}{8\pi\hbar z}\sin\left(\frac{2\tilde{\boldsymbol{\omega}}_{10}z}{c}\right)\frac{\Delta}{2}.
\end{aligned} \tag{62}$$

The same procedure is carried out in the nonretarded limit and the respective reflective coefficients (57) are

$$\begin{aligned}
r_{\mathrm{s,s}}^{\mathrm{nonret}} &= \frac{-\Delta^2}{2(\varepsilon+1)+\Delta^2},\\
r_{\mathrm{p,s}}^{\mathrm{nonret}} &= \frac{-2\Delta}{2(\varepsilon+1)+\Delta^2},\\
r_{\mathrm{p,p}}^{\mathrm{nonret}} &= \frac{2(\varepsilon-1)+\Delta^2}{2(\varepsilon+1)+\Delta^2},\\
r_{\mathrm{s,p}}^{\mathrm{nonret}} &= \frac{-2\Delta}{2(\varepsilon+1)+\Delta^2} = r_{\mathrm{p,s}}^{\mathrm{nonret}}.
\end{aligned} \tag{63}$$

The respective decay rate and resonant frequency shift for the purely axion contribution in the nonretarded limit read

$$\begin{aligned}
\Gamma_{10}^{(1)\mathrm{nonret}}(\varepsilon=1,\theta=\pi) &= -\frac{\mu_0\tilde{\boldsymbol{\omega}}_{10}d^2c}{8\pi\hbar z^2}\frac{\Delta}{2},\\
\delta\boldsymbol{\omega}_{10}^{\mathrm{res,nonret}}(\varepsilon=1,\theta=\pi) &= \frac{\mu_0\tilde{\boldsymbol{\omega}}_{10}d^2c}{16\pi\hbar z^2}\frac{\Delta}{2}.
\end{aligned} \tag{64}$$

Next, we look at general material properties similar to Bi_2Se_3, where we take $\varepsilon=16$ and $\mu=1$ [46]. We compare the case with axion coupling of $\theta=\pi$ and without axion coupling $\theta=0$. Because of the small value of α, the reflective coefficients $r_{\mathrm{p,s}}$ and $r_{\mathrm{s,p}}$ do not have a big impact on the decay rate and the frequency shift. The decay rate and resonant frequency shift in the retarded limit are calculated by inserting the reflective coefficients (61) into Eqs. (33) and (40)

$$\begin{aligned}
\Gamma_{10}^{(1)\mathrm{ret}} &= \frac{\mu_0\tilde{\boldsymbol{\omega}}_{10}^2 d^2}{4\pi\hbar}\left[-\frac{1}{z}\sin\left(\frac{2\tilde{\boldsymbol{\omega}}_{10}z}{c}\right)r_{\mathrm{p,p}}^{\mathrm{ret}}\right.\\
&\quad\left.-\frac{1}{z}\cos\left(\frac{2\tilde{\boldsymbol{\omega}}_{10}z}{c}\right)r_{\mathrm{s,p}}^{\mathrm{ret}}\right],\\
\delta\boldsymbol{\omega}_{10}^{\mathrm{res,ret}} &= \frac{\mu_0\tilde{\boldsymbol{\omega}}_{10}^2 d^2}{8\pi\hbar}\left[\frac{1}{z}\cos\left(\frac{2\tilde{\boldsymbol{\omega}}_{10}z}{c}\right)r_{\mathrm{p,p}}^{\mathrm{ret}}\right.\\
&\quad\left.-\frac{1}{z}\sin\left(\frac{2\tilde{\boldsymbol{\omega}}_{10}z}{c}\right)r_{\mathrm{s,p}}^{\mathrm{ret}}\right].
\end{aligned} \tag{65}$$

The difference in the decay rate and the resonant frequency shift between the cases with and without axion coupling in the retarded limit and for $\Delta\ll 1$ yields

$$\begin{aligned}
\Delta\Gamma_{10}^{(1)\mathrm{ret}} &\equiv \Gamma_{10}^{(1)\mathrm{ret}}(\theta=\pi)-\Gamma_{10}^{(1)\mathrm{ret}}(\theta=0)\\
&= \frac{\mu_0\tilde{\boldsymbol{\omega}}_{10}^2 d^2}{4\pi\hbar z}\cos\left(\frac{2\tilde{\boldsymbol{\omega}}_{10}z}{c}\right)\frac{2\Delta}{(1+n)^2},\\
\Delta\delta\boldsymbol{\omega}_{10}^{\mathrm{res,ret}} &\equiv \delta\boldsymbol{\omega}_{10}^{\mathrm{res,ret}}(\theta=\pi)-\delta\boldsymbol{\omega}_{10}^{\mathrm{res,ret}}(\theta=0)\\
&= \frac{\mu_0\tilde{\boldsymbol{\omega}}_{10}^2 d^2}{8\pi\hbar z}\sin\left(\frac{2\tilde{\boldsymbol{\omega}}_{10}z}{c}\right)\frac{2\Delta}{(1+n)^2}.
\end{aligned} \tag{66}$$

In the limit of $\Delta\ll 1$, the scaling factor for Eq. (66) for $\varepsilon=16$ with respect to the purely axion material in the retarded limit (62) is 4/25.

The decay rate and resonant frequency shift in the nonretarded limit are obtained by inserting Eq. (63) into Eqs. (33) and (40)

$$\begin{aligned}
\Gamma_{10}^{(1)\mathrm{nonret}} &= \frac{\mu_0\tilde{\boldsymbol{\omega}}_{10}^2 d^2}{4\pi\hbar}\left[\frac{c}{2\tilde{\boldsymbol{\omega}}_{10}z^2}r_{\mathrm{s,p}}^{\mathrm{nonret}}+\frac{c^2}{4\tilde{\boldsymbol{\omega}}_{10}^2 z^3}r_{\mathrm{p,p}}^{\mathrm{nonret}}\right],\\
\delta\boldsymbol{\omega}_{10}^{\mathrm{res,nonret}} &= \frac{\mu_0\tilde{\boldsymbol{\omega}}_{10}^2 d^2}{8\pi\hbar}\left[-\frac{c}{2\tilde{\boldsymbol{\omega}}_{10}z^2}r_{\mathrm{s,p}}^{\mathrm{nonret}}-\frac{c^2}{4\tilde{\boldsymbol{\omega}}_{10}^2 z^3}r_{\mathrm{p,p}}^{\mathrm{nonret}}\right].
\end{aligned} \tag{67}$$

The differential effects of the axion coupling on the decay rate and the resonant frequency shift for the nonretarded limit are given by

$$\begin{aligned}
\Delta\Gamma_{10}^{(1)\mathrm{nonret}} &\equiv \Gamma_{10}^{(1)\mathrm{nonret}}(\theta=\pi)-\Gamma_{10}^{(1)\mathrm{nonret}}(\theta=0)\\
&= -\frac{\mu_0\tilde{\boldsymbol{\omega}}_{10}d^2c}{8\pi\hbar z^2}\frac{\Delta}{\varepsilon+1},
\end{aligned}$$

$$\Delta\delta\boldsymbol{\omega}_{10}^{\mathrm{res,nonret}} \equiv \delta\boldsymbol{\omega}_{10}^{\mathrm{res,nonret}}(\theta=\pi) - \delta\boldsymbol{\omega}_{10}^{\mathrm{res,nonret}}(\theta=0) = \frac{\mu_0\tilde{\omega}_{10}d^2c}{16\pi\hbar z^2}\frac{\Delta}{\varepsilon+1}. \tag{68}$$

The respective scaling factor of Eq. (68) with respect to Eq. (64) in the nonretarded limit for $\varepsilon = 16$ is 2/17. The difference in the atomic decay rate and the resonant frequency shift between these two cases follows the same form of the purely axion atomic decay rate and frequency shift and can be compared with that. The scaling factors are gauged in the retarded and nonretarded limit (cf. Figs. 5 and 6).

The nonresonant frequency shift (39) for the topological insulator contains frequency-dependent permeability and permittivity $\varepsilon(i\xi)$ and $\mu(i\xi)$. Without knowing the exact behavior of these quantities we can only approximate the nonresonant frequency shift in the retarded and nonretarded limits. Since the resonant frequency shift always dominates in the retarded limit, we restrict ourselves to gauge the nonretarded limit. For a purely nonreciprocal medium with $\varepsilon = 1$, we obtain

$$\delta\boldsymbol{\omega}_{10}^{\mathrm{nres,nonret}}(\varepsilon=1,\theta=\pi) = \frac{d^2}{16\pi^2\varepsilon_0\hbar z^3}\frac{\Delta}{2}. \tag{69}$$

The result for a general medium reads

$$\delta\boldsymbol{\omega}_{10}^{\mathrm{nres,nonret}} = \frac{\mu_0 d^2}{8\pi^2\hbar}\int_0^\infty d\xi\,\frac{\xi^2}{\xi^2+\tilde{\omega}_{10}^2}e^{-\frac{2\xi z}{c}} \times\left\{-\frac{\xi}{z}r_{\mathrm{s,p}}^{\mathrm{nonret}} - \frac{c}{2z^2}r_{\mathrm{s,p}}^{\mathrm{nonret}} + \frac{c^2\tilde{\omega}_{10}}{4\xi^2 z^3}r_{\mathrm{p,p}}^{\mathrm{nonret}}\right\}. \tag{70}$$

Because of the strong effect of ε compared with Δ the terms with $r_{\mathrm{p,p}}^{\mathrm{nonret}}$ (63) do not have to be considered for the difference between the topological insulator with and without axion coupling. Only $r_{\mathrm{s,p}}^{\mathrm{nonret}}$ remains and is inserted into Eq. (39). For $\xi\to\infty$, $\varepsilon(i\xi)\to 1$. After performing the ξ integral, we obtain the final result for the difference of the nonresonant frequency shift of the topological insulator in the nonretarded limit,

$$\Delta\delta\boldsymbol{\omega}_{10}^{\mathrm{nres,nonret}} \equiv \delta\boldsymbol{\omega}_{10}^{\mathrm{nres,nonret}}(\theta=\pi) - \delta\boldsymbol{\omega}_{10}^{\mathrm{nres,nonret}}(\theta=0) = \frac{d^2}{16\pi^2\varepsilon_0\hbar z^3}\frac{\Delta}{\varepsilon+1}. \tag{71}$$

The total frequency shift of the resonant and nonresonant parts of the topological insulator scales with z^{-1} in the nonretarded limit. An experimental distinction from another material is difficult (cf. Sec. IV B).

In case of an extremely large axion coupling, the reflective coefficients (57) reduce to the values $r_{\mathrm{s,s}} = -1$ and $r_{\mathrm{p,p}} = 1$. Both the decay rates, the resonant frequency shift, and the nonresonant frequency shift approximate the results of the perfectly conducting mirror; cf. Figs. 2 and 3.

Note that for each of the interacting time-reversal-symmetry-breaking subsystems, atom and medium, there are two possible choices regarding their internal sense of time. For the atom, they correspond to clockwise versus counterclockwise circular dipole transitions and can be related to one another via $\mathbf{d}\to\mathbf{d}^*$. For the medium, the two possible internal senses of time are related via $\Delta\to-\Delta$ or $r_{\mathrm{s,p}}$, $r_{\mathrm{p,s}}\to -r_{\mathrm{s,p}}, -r_{\mathrm{p,s}}$. We thus have four possible combinations of t-odd atoms interacting with nonreciprocal media. The other three possible combinations can be obtained from the particular choice considered here by changing the internal arrow of time in atom, medium or both, where each such change reverses the signs of frequency shift and body-assisted decay rate.

Due to the internal connection between the frequency shift and the Casimir–Polder force, one can also switch from an attractive to a repulsive force between atom and medium.

V. SUMMARY

We have applied macroscopic QED to derive expressions for the Casimir–Polder frequency shift and spontaneous decay rate for nonreciprocal media, which violate Lorentz's reciprocity principle and therefore break time-reversal symmetry. Consequently, real and imaginary parts of the Green's tensor for nonreciprocal media have to be redefined by using the adjoint tensor instead of the complex-conjugate one.

Based on the interaction Hamiltonian between the atom, the field and the nonreciprocal medium, an expression for the electric field has been obtained in two alternative ways. First, noise currents can be quantized directly yielding one set of field operators for the combined electric and magnetic fields. According to the second approach the noise currents can be divided into contributions for the polarization and the magnetization giving rise to cross correlations between electric and magnetic fields. The result for the electric field has enabled us to study the internal atomic dynamics. By making use of the redefined real and imaginary parts of a tensor, we obtain general expressions for the atomic decay rate and the frequency shift, which can be split into a resonant and a nonresonant contribution, representing generalizations for nonreciprocal media.

As an example, we have investigated the decay rate and frequency shift for a two-level atom with circularly polarized dipole moments in order to be able to detect the broken time-reversal symmetry. First, a perfectly conducting mirror has been compared with a perfectly reflecting nonreciprocal mirror yielding different polynomial scaling behavior. Whereas the nonresonant frequency shift of the perfectly conducting mirror decays with z^{-4} in the retarded limit, it scales with z^{-5} in case of the perfectly reflecting nonreciprocal mirror. In the nonretarded limit both scale with z^{-3}. As for the resonant frequency shift, there is a z^{-1} behavior for both materials in the retarded limit and in the nonretarded limit they differ again: the perfectly conducting mirror scales with z^{-3}, the perfectly reflecting nonreciprocal mirror with z^{-2}.

Second, we have investigated a time-reversal-symmetry-broken topological insulator, whose electromagnetic properties are described by an axion coupling and whose reflective coefficients depend on the wave vector. Due to the small impact of the axion part, we have restricted ourselves to a medium of pure axion behavior by setting $\varepsilon = 1$ and compared this to the difference quantities between included axion coupling and without axion coupling for a material similar to Bi_2Se_3. We find a qualitatively similar behavior and determine scaling factors between the two cases in the retarded and nonretarded

limits. Finally, we can switch the sign of the decay rate and the frequency shift of the topological insulator both by reversing the direction of the oscillating dipole moments and by changing the sign of the axion coupling. This opens the door for switching between attractive and repulsive Casimir–Polder forces.

ACKNOWLEDGMENTS

We would like to thank A. Sihvola, Tobias Brünner, and Robert Bennett for discussions. This work was supported by the German Research Foundation (DFG, Grants No. BU 1803/3-1 and No. GRK 2079/1). S.Y.B. is grateful for support by the Freiburg Institute of Advanced Studies.

[1] H. Casimir and D. Polder, Phys. Rev. **73**, 360 (1948).
[2] H. B. G. Casimir, Proc. K. Ned. Acad Wet. **51**, 793 (1948).
[3] S. Y. Buhmann, *Dispersion Forces I - Macroscopic Quantum Electrodynamics and Ground-State Casimir, Casimir–Polder and van der Waals Forces* (Springer, Berlin, Heidelberg, 2012).
[4] S. Y. Buhmann, *Dispersion Forces II - Many-Body Effects, Excited Atoms, Finite Temperature and Quantum Friction* (Springer, Berlin, Heidelberg, 2012).
[5] J. M. Wylie and J. E. Sipe, Phys. Rev. A **30**, 1185 (1984).
[6] J. M. Wylie and J. E. Sipe, Phys. Rev. A **32**, 2030 (1985).
[7] H. T. Dung, L. Knöll, and D.-G. Welsch, Phys. Rev. A **57**, 3931 (1998).
[8] S. Y. Buhmann, L. Knöll, D.-G. Welsch, and H. T. Dung, Phys. Rev. A **70**, 052117 (2004).
[9] S. Y. Buhmann and D.-G. Welsch, Prog. Quantum Electron. **31**, 51 (2007).
[10] S. Scheel and S. Y. Buhmann, Acta Phys. Slovaca **58**, 675 (2008).
[11] B.-S. Skagerstam, P. K. Rekdal, and A. H. Vaskinn, Phys. Rev. A **80**, 022902 (2009).
[12] W. C. Chew, *Waves and Fields in Inhomogeneous Media*, Series on Electromagnetic Waves (IEEE Press, New York, 1995).
[13] L. Knöll, S. Scheel, and D. G. Welsch, in *Coherence and Statistics of Photons and Atoms*, edited by J. Perina (Wiley, New York, 2001).
[14] C. Eberlein and R. Zietal, Phys. Rev. A **86**, 062507 (2012).
[15] J. Xu, M. Alamri, Y. Yang, S.-Y. Zhu, and M. S. Zubairy, Phys. Rev. A **89**, 053831 (2014).
[16] C. Henkel and K. Joulain, Europhys. Lett. **72**, 929 (2005).
[17] J. A. Crosse, S. A. Ellingsen, K. Clements, S. Y. Buhmann, and S. Scheel, Phys. Rev. A **82**, 010901 (2010).
[18] V. Yannopapas, J. Phys.: Condens. Matter **18**, 6883 (2006).
[19] M. Thiel, M. S. Rill, G. von Freymann, and M. Wegener, Adv. Mater. **21**, 4680 (2009).
[20] D. V. Guzatov and V. V. Klimov, Quantum Electron. **44**, 1112 (2014).
[21] D. V. Guzatov and V. V. Klimov, Quantum Electron. **44**, 873 (2014).
[22] V. V. Klimov, D. V. Guzatov, and M. Ducloy, Europhys. Lett. **97**, 47004 (2012).
[23] D. Guzatov, V. Klimov, and N. Poprukailo, J. Exp. Theor. Phys. **116**, 531 (2013).
[24] L. Onsager, Phys. Rev. **37**, 405 (1931).
[25] H. A. Lorentz, Verhandelingen en bijdragen uitgegeven door de Afeeling Natuurkunde, Koninklijke Nederlandse Akademie van Wetenschappen te Amsterdam **4**, 176 (1896).
[26] S. Y. Buhmann, D. T. Butcher, and S. Scheel, New J. Phys. **14**, 083034 (2012).
[27] S.-Q. Shen, Natl. Sci. Rev. **1**, 49 (2014).
[28] B. A. Bernevig, T. L. Hughes, and S. C. Zhang, Science **314**, 1757 (2006).
[29] M. Z. Hasan and C. L. Kane, Rev. Mod. Phys. **82**, 3045 (2010).
[30] H. Zhang, L. C. X., X. L. Qi, X. Dai, Z. Fang, and S. C. Zhang, Nat. Phys. **5**, 438 (2009).
[31] X.-L. Qi, R. Li, J. Zang, and S.-C. Zhang, Science **323**, 1184 (2009).
[32] Y. L. Chen, J.-H. Chu, J. G. Analytis, Z. K. Liu, K. Igarashi, H.-H. Kuo, X. L. Qi, S. K. Mo, M. R. G., D. H. Lu, M. Hashimoto, T. Sasagawa, S. C. Zhang, I. R. Fisher, Z. Hussain, and Z. X. Shen, Science **329**, 659 (2010).
[33] J. Maciejko, X.-L. Qi, H. D. Drew, and S.-C. Zhang, Phys. Rev. Lett. **105**, 166803 (2010).
[34] F. Wilczek, Phys. Rev. Lett. **58**, 1799 (1987).
[35] A. G. Grushin and A. Cortijo, Phys. Rev. Lett. **106**, 020403 (2011).
[36] M.-C. Chang and M.-F. Yang, Phys. Rev. B **80**, 113304 (2009).
[37] Z. W. Zuo, D. B. Ling, L. Sheng, and D. Y. Xing, Phys. Lett. A **377**, 2909 (2013).
[38] F. R. Prudêncio, S. A. Matos, and C. R. Paiva, IEEE Trans. Antennas Propag. **62**, 4637 (2014).
[39] J. A. Crosse, arXiv:1510.06130.
[40] F. S. S. Rosa, D. A. R. Dalvit, and P. W. Milonni, Phys. Rev. Lett. **100**, 183602 (2008).
[41] F. S. S. Rosa, D. A. R. Dalvit, and P. W. Milonni, Phys. Rev. A **78**, 032117 (2008).
[42] R. Zhao, J. Zhou, T. Koschny, E. N. Economou, and C. M. Soukoulis, Phys. Rev. Lett. **103**, 103602 (2009).
[43] L. Chen and S. Wan, Phys. Rev. B **84**, 075149 (2011).
[44] L. M. Woods, D. A. R. Dalvit, A. Tkatchenko, P. Rodriguez-Lopez, A. W. Rodriguez, and R. Podgornik, Rev. Mod. Phys. **88**, 045003 (2016).
[45] T. Cysne, W. J. M. Kort-Kamp, D. Oliver, F. A. Pinheiro, F. S. S. Rosa, and C. Farina, Phys. Rev. A **90**, 052511 (2014).
[46] J. A. Crosse, S. Fuchs, and S. Y. Buhmann, Phys. Rev. A **92**, 063831 (2015).
[47] P. Curie, J. Phys. Theor. Appl. **3**, 393 (1894).
[48] G. Barton, Proc. R. Soc. London, Ser. A **320**, 251 (1970).
[49] G. Barton, Proc. R. Soc. London, Ser. A **367**, 117 (1979).
[50] *Advances in Atomic, Molecular, and Optical Physics*, edited by D. Bates and B. Bederson (Academic Press, Inc., San Diego, 1991), Vol. 28.
[51] A. Sihvola and I. V. Lindell, Ann. Phys. (Berlin, Ger.) **17**, 787 (2008).
[52] I. V. Lindell and A. H. Sihvola, J. Electromagnet. Wave. **19**, 861 (2005).
[53] I. V. Lindell and A. H. Sihvola, IEEE Trans. Antennas Propag. **53**, 3005 (2005).
[54] A. H. Sihvola, A. Viitanen, I. Lindell, and S. Tretyakov, *Electromagnetic Waves in Chiral and Bi-Isotropic Media* (Artech House Antenna Library, Boston, London, 1994).
[55] G. Song, J.-P. Xu, and Y.-P. Yang, EPL **105**, 64001 (2014).